S1 Overview of supplementary material

This Supplement documents the tests, comparison tables, and machine-readable products used to define the climate information retained in the Kiso *Chamaecyparis* chronology. The main manuscript treats rural Chubu pNov–Apr temperature predicted from RWI(t) as the authoritative primary specification. Alternative seasons and the adjacent-ring carry-over formulation are sensitivity analyses rather than model-selection alternatives.

The evidence hierarchy is explicit. Annual split-period verification and the G21 high-pass results are formal out-of-sample tests. G21 and G51 low-pass verification is reported as not evaluable because split-specific filtering and effective-sample-size requirements leave no valid split. Smoothed reconstruction curves remain useful as persistence summaries, but their slow variability is supported by synthetic signal-retention and standardization-robustness tests, not by formal low-pass predictive-skill statistics.

Section S1 provides this overview. Section S2 describes chronology components, sample depth, running SSS, and the selected standardization. Section S3 reports calibration, leakage-safe frequency-dependent verification, and synthetic signal retention. Section S4 presents the carry-over test and descriptive smoothed-mean contrasts. Section S5 provides documentary snowfall, SST, and winter-monsoon context. Section S6 compares Takayama with the rural Chubu target. Section S7 inventories the supplementary and run-scoped audit products, including Table 3 method v5.3.

JMA denotes the Japan Meteorological Agency, and RWI denotes ring-width index. SSS denotes subsample signal strength, RE reduction of error, and CEff coefficient of efficiency. G11, G21, and G51 denote nominal Gaussian smoothing scales rather than sharp spectral cutoffs. Visual structure in smoothed or decomposed records is not treated as evidence of periodic forcing, formal climate regimes, or precise centennial amplitude.

S2 Chronology signal strength and standardization

Figure S1 separates the final chronology from its component low-frequency series. This distinction is important because the record is assembled from living trees, archaeological coffin wood, building timbers, and buried wood whose overlap and replication change through time. Chronology length alone does not show whether a particular interval is well supported.

The living-tree clusters A–C are historical cohort classes rather than species or climate-response groups. Their boundaries use the earliest measured ring, which is only a proxy for cohort age because pith may be missing and sampling height varies. Cluster A begins after 1708, cluster B between the 1664–1665 protected-forest benchmark and 1708, and cluster C before 1665. These dates bracket major stages in early-modern Kiso forest regulation (Tokoro, 1980; Yonenobu et al., 2026).

All three living-tree clusters are Hinoki-dominated and include additional series relative to Ohyama et al. (2026a). Cluster A contains 241 Hinoki and 18 Sawara series, cluster B contains 40 Hinoki and 3 Sawara, and cluster C contains 35 Hinoki and 1 Sawara. The labels therefore do not represent a Hinoki versus Sawara classification. The minor Sawara component was retained in the regional chronology because it crossdates coherently within the Kiso *Chamaecyparis* framework, but species-specific climate sensitivity was not modeled separately.

Cluster D contains the archaeological coffin sites Minamimotomachi (13MM), Hachobori-sanchome (13HT), and Mirokuji-ato (13MR), and cluster F contains the Tohyama buried-forest material (20TY); these two clusters were not expanded for the present climate-analysis dataset. Cluster E includes historical building timbers, including added Chiko-ji/Yakushi-do material (20IK). The overlap component E_in_D consists entirely of newly added Chiko-ji/Yakushi-do material used to bridge component chronologies and is not an independent material class.

Running SSS was calculated from the number of contributing series, n, and the mean interseries correlation, $\bar{r}$, following Wigley et al. (1984):

$$\mathrm{SSS} = \frac{n\bar{r}}{1 + (n-1)\bar{r}}.$$

The values reported here use centered 51-year windows. SSS $= 0.85$ is a conventional screening value, not a physical or statistically unique threshold. The first isolated window exceeding 0.85 is centered at 119 CE, and a record-length-oriented interpretation could reasonably begin there. The main manuscript instead adopts 259 CE as a conservative author-defined boundary for formal climatic interpretation because early replication and common-signal support are lower and less continuous. This boundary is not an estimated changepoint. SSS also shows local dips after 259 CE, so the complete running series is retained in machine-readable Table S1c for interval-specific assessment.

The primary standardization is labeled RWdiv SPL150. RWdiv indicates ratio standardization, and SPL150 identifies the 150-year cubic smoothing spline used for the relevant historical, archaeological, and buried-wood components. Cluster C was treated with a second-order polynomial bridge to 1730 CE because its cohort-level growth curve has pronounced curvature. A quadratic term was also used to summarize curved Type-2 trajectories in Kiso Nezuko (Yonenobu et al., 2026). Here, however, the polynomial is only a low-order detrending and bridging device; it does not assign cluster C to the Nezuko Type-2 ecological class.

Table S1 summarizes the chronology-strength information needed to interpret the reconstruction. The full annual series and material inventories are supplied as machine-readable Tables S1a–S1g.

Table S1. Chronology strength and standardization summary.

Item	Summary
Numerical chronology span	-156 to 2025 CE in signed-year files.
Main interpretation interval	259–2025 CE, with annual SSS retained for interval-specific checks.
Maximum sample depth	331 measured series in the best-replicated interval.
Running SSS	Mean 0.884 and maximum 0.995; early low-replication windows are retained as lower-confidence output.
Primary standardization	RWdiv SPL150, with group-specific standardization and a polynomial bridge for cluster C.
Main caution	SSS measures common signal among tree-ring series, not climate-reconstruction skill by itself.
Machine-readable files	Tables S1a–S1g provide chronology values retained for audit, sample depth, running SSS, component chronologies, material inventories, and summary metadata.

S3 Calibration, leakage-safe verification, and signal retention

Table S2. Seasonal target and predictor roles.

Item	Role	Interpretation
pNov–Apr temperature	Authoritative seasonal target	Regional Chubu rural/background cold-season anomaly used for the primary reconstruction.
FMA temperature	Legacy seasonal comparison	Provides continuity with the earlier FMA reconstruction; it is not co-primary.
MAM temperature	Seasonal-domain sensitivity	Documents adjacent spring response; it is not reconstructed as a primary product.
JAS and JASO temperature	Warm-season sensitivities	High-frequency comparison products; no robust low-pass claim is made.
RWI(t)	Primary predictor	Current-year standardized ring-width index used in the authoritative model.
mean[RWI(t), RWI($t+1$)]	Carry-over sensitivity	Constrained adjacent-ring test of predictor indexing; it does not use future climate information.

S3.1 Annual calibration and verification

The primary model uses the regional Chubu rural/background pNov–Apr anomaly and RWI(t). Full-period calibration over 1912–2023 ($n = 112$) gives $r = 0.416$, adjusted $R^2 = 0.165$, RMSE $= 0.789\,°\mathrm{C}$, Durbin–Watson $= 1.777$, and residual AR1 $= 0.045$. The carry-over sensitivity gives $r = 0.368$, adjusted $R^2 = 0.128$, and RMSE $= 0.807\,^\circ$C.

Seven annual splits test early-to-late, late-to-early, and modern-tail behavior. For the primary model, RE and CEff are positive in six of seven splits; mean RE is 0.175, mean CEff 0.099, minimum CEff -0.068, and median verification $r = 0.376$. The carry-over formulation gives five positive RE/CEff splits and mean CEff $= -0.062$. Test-level statistics are retained in the disclosed CSV files; no split is omitted because its value is unfavorable.

S3.2 Leakage-safe frequency-dependent verification

For each split and scale, calibration and verification segments were transformed independently. Centered Gaussian kernels were prohibited from crossing split boundaries, incomplete edge values were excluded, and formal evaluation required a Bretherton effective sample size of at least eight (Bretherton et al., 1999). This prevents information from the verification segment from entering the calibration transformation.

Annual results remain evaluable in all seven splits. For the primary model, G21 high-pass results are evaluable in four splits and all four have positive RE and CEff; mean CEff is 0.127 and median verification $r = 0.341$. The carry-over G21 high-pass results are also positive in the four evaluable splits, but have lower mean CEff (0.049) and median r (0.214).

No G21 low-pass split meets the effective-sample-size requirement, and no G51 low-pass split has sufficient transformed support and effective sample size. Raw diagnostic values remain archived where calculable, but are not summarized as predictive skill. In particular, the absence of an evaluable result is not converted into a positive or negative low-frequency verification claim.

Table S3. Authoritative calibration and verification summary.

Evidence	Primary RWI(t)	Carry-over sensitivity	Interpretation
Full calibration	$r = 0.416$; adjusted $R^2 = 0.165$; RMSE $= 0.789\,^\circ$C	$r = 0.368$; adjusted $R^2 = 0.128$; RMSE $= 0.807\,^\circ$C	Supports the simpler current-ring model.
Annual CV	6/7 positive CEff; mean 0.099	5/7 positive CEff; mean -0.062	Formal out-of-sample evidence.
G21 high-pass	4/4 evaluable splits positive; mean CEff 0.127	4/4 evaluable splits positive; mean CEff 0.049	Formal evidence for variability shorter than the nominal 21-year scale.
G21 low-pass	0/7 formally evaluable	0/7 formally evaluable	No predictive-skill claim.
G51 low-pass	0/7 formally evaluable	0/7 formally evaluable	Descriptive smoothing only.

S3.3 Synthetic signal-retention test

Known periodic inputs were passed through the chronology-processing workflow. For imposed signal $s_P(t)$ and recovered component $\hat{s}_P(t)$, shape and timing are summarized by $r_P = \mathrm{cor}\{s_P(t), \hat{s}_P(t)\}$; the slope of recovered on imposed signal is the gain. These tests diagnose the processing system and are not independent climate validation.

Median recovery r is 0.988, 0.986, 0.983, and 0.972 for 11-, 21-, 31-, and 51-year inputs, with gain 0.988, 0.977, 0.960, and 0.909 and zero median phase lag. At 75 and 101 years, recovery remains coherent ($r = 0.956$ and 0.925) but gain falls to 0.816 and 0.671. At 150 and 200 years, recovery declines to 0.786 and 0.559 and gain to 0.383 and 0.196. The workflow therefore supports cautious interpretation of multidecadal timing and broad shape, not precise centennial amplitude.

Table S4. Synthetic signal-retention summary.

Period	Median r	Median gain	Interpretation
11 yr	0.988	0.988	Timing and amplitude well retained.
21 yr	0.986	0.977	Timing and amplitude well retained.
31 yr	0.983	0.960	Timing and amplitude well retained.
51 yr	0.972	0.909	Multidecadal timing retained with modest attenuation.
75 yr	0.956	0.816	Coherent but attenuated.
101 yr	0.925	0.671	Coherent with substantial amplitude loss.
150–200 yr	0.786–0.559	0.383–0.196	Not used for precise centennial amplitude.

S3.4 Seasonal target variables and multiresolution products

FMA, MAM, JAS, and JASO are retained to document proxy-domain limits and to support future comparison. They are not co-primary reconstructions. Earlier frequency-band summaries that filtered a complete series before splitting are superseded by the leakage-safe primary-model analysis above. Multiresolution products for alternative seasonal variables remain descriptive records of reconstructed variance; they are not used as verification, model selection, or forcing evidence.

S4 Carry-over sensitivity and smoothed-mean contrasts

The carry-over predictor is

$$\mathrm{RWI}_{\mathrm{co}}(t) = \frac{\mathrm{RWI}(t) + \mathrm{RWI}(t+1)}{2}.$$

The $t+1$ label follows meteorological-year assignment and does not represent future climate information. Equal weights keep the comparison deliberately constrained.

Over 1912–2023, its calibration is weaker than the primary model ($r = 0.368$ versus 0.416; adjusted $R^2 = 0.128$ versus 0.165; RMSE $= 0.807$ versus 0.789 °C). Annual split verification also favors the primary model: mean CEff is -0.062 for the carry-over formulation and 0.099 for RWI(t). G21 high-pass results are positive for all four evaluable splits in both models, but mean CEff is lower for carry-over (0.049 versus 0.127).

The reconstructed series nevertheless remain similar after smoothing. Annual agreement is $r = 0.867$, rising to 0.995 at G21 and 0.999 at G51, with smoothed RMSE differences of 0.016 and 0.007 °C. These comparisons show that the broad smoothed curve is insensitive to this constrained predictor change; they do not constitute low-pass out-of-sample verification.

Table S5. Carry-over comparison.

Scale	Correlation	RMSE difference (°C)	Interpretation
Annual	0.867	–	Calibration and annual verification favor RWI(t).
G21 smoothed	0.995	0.016	Persistence summary is nearly unchanged.
G51 smoothed	0.999	0.007	Broad shape is insensitive to the constrained formulation.

If $\hat{T}_k(t)$ is a reconstruction smoothed at scale k, a local contrast around year c is summarized as

$$\Delta_k(c) = \overline{\hat{T}_k}(t > c) - \overline{\hat{T}_k}(t < c),$$

using predefined windows. Large contrasts around approximately 769, 1006, 1477, and 1625 CE are retained as descriptive curve features. They were not used in Table 3 v5.3 candidate generation or retention, and no correspondence between these dates and a physical regime is inferred.

Table S6. Smoothed-mean contrast summary.

Approximate year	Scale(s)	Interpretation
769 CE	G21/G51	Large descriptive contrast; not a retained climate interval.
1006 CE	G21/G51	Large descriptive contrast; not a retained climate interval.
1477 CE	G21/G51	Curve diagnostic only; independent of Table 3 screening.
1625 CE	G21/G51	Curve diagnostic only; no forcing or regime claim.

S5 Documentary snowfall, SST, and winter-monsoon context

The Kawanishi snowfall-rate series are based on daily weather entries in the Takeda Gen'emon diary. Hirano et al. (2012) used the diary's December–February snowfall ratio to reconstruct winter temperature from 1830/31 onward. Hirano et al. (2025) subsequently placed its February–April snowfall ratio in a longer Tohoku documentary framework by linking Kawanishi with Hirosaki diary records and JMA Yamagata observations. The present analysis builds on those published interpretations but recalculates the relationships with the Kiso reconstruction and the instrumental series listed in the machine-readable snowfall-context files.

The Kawanishi analysis has two stages. First, documentary snowfall rates are compared with JMA Yamagata observations to establish whether they represent cold conditions, snow occurrence, or precipitation more generally. Second, they are compared with reconstructed Kiso pNov–Apr temperature. This ordering is important: the instrumental bridge evaluates the documentary variable, whereas the Kiso comparison provides regional climate context.

For 1890–1980, Kawanishi DJF snowfall rate correlates with Yamagata mean temperature at $r = -0.743$ annually, -0.868 at G11, and -0.904 at G21. During the shorter 1954–1980 snowfall-amount overlap, the correlations are 0.701 annually and 0.920 at G21. FMA snowfall rate gives an annual correlation of -0.636 with mean temperature for 1890–1980 and 0.818 with snowfall amount for 1953–1980. These results establish a strong local cold-snow interpretation for the documentary rates.

The full documentary overlap with Kiso is 150 years, but the direct association is weaker. Annual correlations with reconstructed temperature are -0.259 for DJF and -0.210 for FMA; the largest full-overlap smoothed value is $r = -0.329$ for FMA at G11. Relations are stronger during the instrumental subperiod, as documented in the machine-readable snowfall-context files, but those shorter comparisons are not used as independent validation. The diary series is local, the Kiso record is a regional temperature proxy, and snowfall depends on moisture as well as temperature.

Filtering increases serial dependence, so the smoothed coefficients are reported descriptively rather than tested as if filtered values were independent observations. The machine-readable snowfall-context files retain the JMA bridge, partial correlations, lagged Kiso–snowfall comparisons, split periods, and period–scale comparisons.

Figure S6 places the reconstruction within broader winter climate variability. Earlier central- and northeast-Asian tree-ring studies reconstructed February–April or spring temperature and compared the results with documentary evidence, regional proxies, or East Asian winter-monsoon dynamics (Yonenobu and Eckstein, 2006; Zhu et al., 2009; Ohyama et al., 2013). The Changbai Mountain February–April reconstruction, in particular, showed inverse correlations with instrumental and proxy-based winter-monsoon intensity records (Zhu et al., 2009). A later gridded reconstruction based on 260 temperature-sensitive chronologies provides broader DJF winter-temperature context across East Asia (Song et al., 2021). The present analysis adds separate comparisons with COBE-SST2 (Hirahara et al., 2014), the D'Arrigo East Asian winter monsoon index (D'Arrigo et al., 2005b), and the D'Arrigo reconstructed Siberian High index (D'Arrigo et al., 2005a). The later observation-based literature is used to interpret these historical comparisons, not as a replacement analytical dataset.

The preselected central/eastern Japan Sea SST box gives pNov–Apr correlations of 0.504 annually, 0.742 at G11, and 0.833 at G21. FMA values are 0.510, 0.756, and 0.853. These coefficients indicate strong decadal covariability during the instrumental overlap. This result is consistent with the broader background-temperature analysis of Katata et al. (2025), which related rural/background temperature variability to large-scale oceanic context. Control boxes over the western North Pacific and the Kuroshio region also show substantial smoothed relationships, however. The Japan Sea result is physically plausible but is not uniquely indicative of a local SST mechanism.

The East Asian winter monsoon is a three-dimensional circulation system involving the Siberian High and Aleutian Low at the surface, lower-tropospheric coastal northerlies, the East Asian trough in the middle troposphere, and the upper-level East Asian jet (Takaya and Nakamura, 2013; Miao and Wang, 2020; Ma and Chen, 2021). Its variability is also associated with Eurasian and western Pacific planetary-wave and teleconnection patterns (Takaya and Nakamura, 2013). These components need not vary coherently at decadal time scales (Miao and Wang, 2020). The late-20th-century weakening of Siberian High intensity (Panagiotopoulos et al., 2005) and its subsequent rapid recovery (Jeong et al., 2011) further demonstrate that the behavior of this single center of action is temporally variable.

Within this framework, central-Japan temperature, Japan Sea-side snowfall, and regional SST can covary without being controlled by a single index. The D'Arrigo winter monsoon index has a moderate inverse G21 association with Kiso ($r = -0.505$), whereas the D'Arrigo reconstructed Siberian High index alone shows little direct correspondence. Kiso is therefore interpreted as a downstream cold-season temperature record embedded in the broader integrated winter-monsoon system, not as a reconstruction of Siberian High intensity.

Table S7. Documentary, SST, and winter-monsoon context summary.

Comparison	Result and interpretation
Kawanishi DJF snowfall rate vs JMA Yamagata temperature	$r = -0.743$ annually, -0.868 at G11, and -0.904 at G21. These values establish the local cold-snow meaning of the documentary snowfall-rate series.
Kawanishi snowfall rate vs Kiso reconstruction	Annual correlations are $r = -0.259$ for DJF and -0.210 for FMA. The association provides weak to moderate regional context, not independent validation.
Central/eastern Japan Sea SST vs Kiso pNov–Apr	$r = 0.504$ annually, 0.742 at G11, and 0.833 at G21. This indicates strong smoothed air–sea covariability, but not a unique local SST mechanism.
East Asian winter monsoon index	The G21 association is moderately inverse ($r = -0.505$), consistent with a downstream winter-monsoon setting but not uniquely diagnostic of one circulation component.
Siberian High index	Direct correspondence is weak; an individual center of action can diverge from other components of the integrated monsoon, and Kiso is not interpreted as a direct Siberian High reconstruction.

The machine-readable SST/circulation files associated with Table S7 report the full SST boxes and circulation-index results. The comparisons are used to assess physical consistency and geographic context, not to infer oceanic forcing, atmospheric attribution, or independent validation. This restriction is important because relationships among winter-monsoon components and between ENSO and the winter monsoon vary with time scale and background state (Miao and Wang, 2020; Ma and Chen, 2021, 2023).

S6 Takayama and regional Chubu rural/background target comparison

Table S8. Takayama–regional Chubu rural/background comparison.

Item	Summary
Chubu product	Eight rural/background stations selected to reduce urbanization-related influence; “chubu7” is an internal regional code, not a station count.
Series history	The regional Chubu product is described by Katata et al. (2025); the 1916–2023 monthly dataset is archived by Katata and Fujibe (2026). A subsequent update extends the monthly series back to 1911. The derived seasonal values used here are included in the restricted-review archive with provider approval.
Regression direction	The dependent and predictor variables are stated explicitly because OLS slopes are direction-dependent.
Mean-level display	A season-specific additive alignment is used; correlation, variance, OLS slope within a specified direction, and regression-residual RMSE with an intercept are invariant to that shift, whereas the mean difference and intercept are alignment-dependent.
Machine-readable files	Tables S8g–S8i provide regression statistics, seasonal values, and raw Takayama monthly climatology.

Figure S7 compares available source values for the local and regional target definitions over 1911–2025. The product methods are described by Katata et al. (2025), and the archived 1916–2023 monthly dataset is available as Katata and Fujibe (2026). The comparison uses a subsequent update that extends the monthly series back to 1911 and includes later source values through 2025. The authoritative reconstruction calibration nevertheless uses only the 112 complete pNov–Apr seasons from 1912 through 2023. The derived seasonal series used here are included in the password-protected reviewer archive referenced in the main manuscript. A season-specific additive alignment places the regional anomaly series on a comparable display scale with raw Takayama. The comparison therefore separates shared variability from mean-level alignment and does not treat the plotted mean difference as a direct urban-bias estimate.

Takayama and the Chubu product share much of their interannual variability, but their levels, amplitudes, and error structures differ. These differences are consistent with the rural/background design of the Chubu product (Katata et al., 2023, 2025), while station composition, elevation, exposure, local topography, and alignment also contribute. The comparison is consequently a target-definition diagnostic, not a causal attribution of all differences to urbanization.

The regional Chubu rural/background series is preferred for the primary model because it is constructed from eight stations selected to reduce urbanization-related influence and reduces dependence on one station history. Raw Takayama remains a valuable local and legacy benchmark. Tables S8g–S8i preserve the exact comparison in machine-readable form.

S7 Supplementary tables and disclosed data

Printed Tables S1–S9 provide compact summaries, while machine-readable CSV files preserve annual values, individual splits, filter support, station and grid statistics, and method metadata. The authoritative verification products are the annual split results and summary (`annual_split_verification.csv` and `annual_split_verification_summary.csv`), the frequency-dependent split results and summary (`frequency_cv_split_results.csv` and `frequency_cv_summary.csv`), and the filter-support table (`frequency_cv_filter_support.csv`). The latter records the exact support window and guard exclusion for each transformed value.

Table S1 summarizes chronology strength. Table S2 lists seasonal target variables and their role. Table S3 gives authoritative calibration and leakage-safe verification. Table S4 gives synthetic signal retention. Tables S5 and S6 summarize carry-over and descriptive curve contrasts. Tables S7 and S8 cover external winter context and target-series comparison. Table S9 inventories public-release and audit products.

The rule-based interval audit is tied to Table 3 method v5.3 and to the frozen authoritative run identified in the repository manifest. Disclosed files include the full candidate table, retained-interval audit, decision diagnostics, candidate-year flags, SSS-window assignment audit, method manifest, figure manifest, workflow state, and SHA-256 identifiers for the production uncertainty cache and G51 ensemble descriptor. All candidates are disclosed, including the rejected 1458–1473 CE lower-tail interval and the retained 1999–2015 CE upper-tail interval.

The production uncertainty method is u2.0 with 2000 draws and no calibration-only fallback. Its stated scope includes calibration-parameter and four-member standardization uncertainty, but not source-group removal, species exclusion, or individual-series resampling. Public package metadata must retain this boundary and must not imply that omitted uncertainty sources were sampled.

Table S9. Review-stage and post-acceptance reproducibility inventory.

Product group	Review/post-acceptance availability	Release scope
Final annual RWI and year-aligned calibration table	Restricted-review archive; DOI repository after acceptance	Reproduces the authoritative climate model from the final chronology onward.
Reconstruction, uncertainty, annual CV, and frequency CV	Restricted-review archive; DOI repository after acceptance	Includes test-level results, filter support, and explicit non-evaluability of low-pass splits.
Running SSS, sample depth, component chronologies, and Table 3 v5.3 audit	Restricted-review archive; DOI repository after acceptance	Includes all candidates, decisions, workflow metadata, and hashes.
Spatial, target-comparison, documentary-context, and figure-source tables	Included where redistribution permits	Derived tables are disclosed; full annual Kawanishi and D'Arrigo source series are excluded; third-party data retain provider terms.
Scripts, tests, dictionaries, manifests, checksums, and session information	Restricted-review archive; DOI repository after acceptance	Supports reproduction of all manuscript-facing climate analyses from the final RWI onward.
Provenance and dating mean curves	Public externally	Available with Ohyama et al. (2026a) and Ohyama et al. (2026b).
Individual raw ring-width measurements and restricted sample-level provenance	Not in this release	Requests are subject to coauthor agreement and provenance constraints.

The external-data and disclosure inventory is supplied in the repository metadata directory. The final archive should include manuscript figures and tables, source data where permitted, the R0 authoritative-number registry, run manifests, checksums, and session/package information. The final annual RWI and all downstream climate-analysis inputs will be included in the accompanying repository; individual raw measurements and restricted sample-level provenance remain subject to the data-sharing statement in the main manuscript. The password-protected reviewer archive is available at the URL given in the main manuscript; after acceptance, the Tohoku University repository record will be assigned a DOI and preserved as the permanent release.

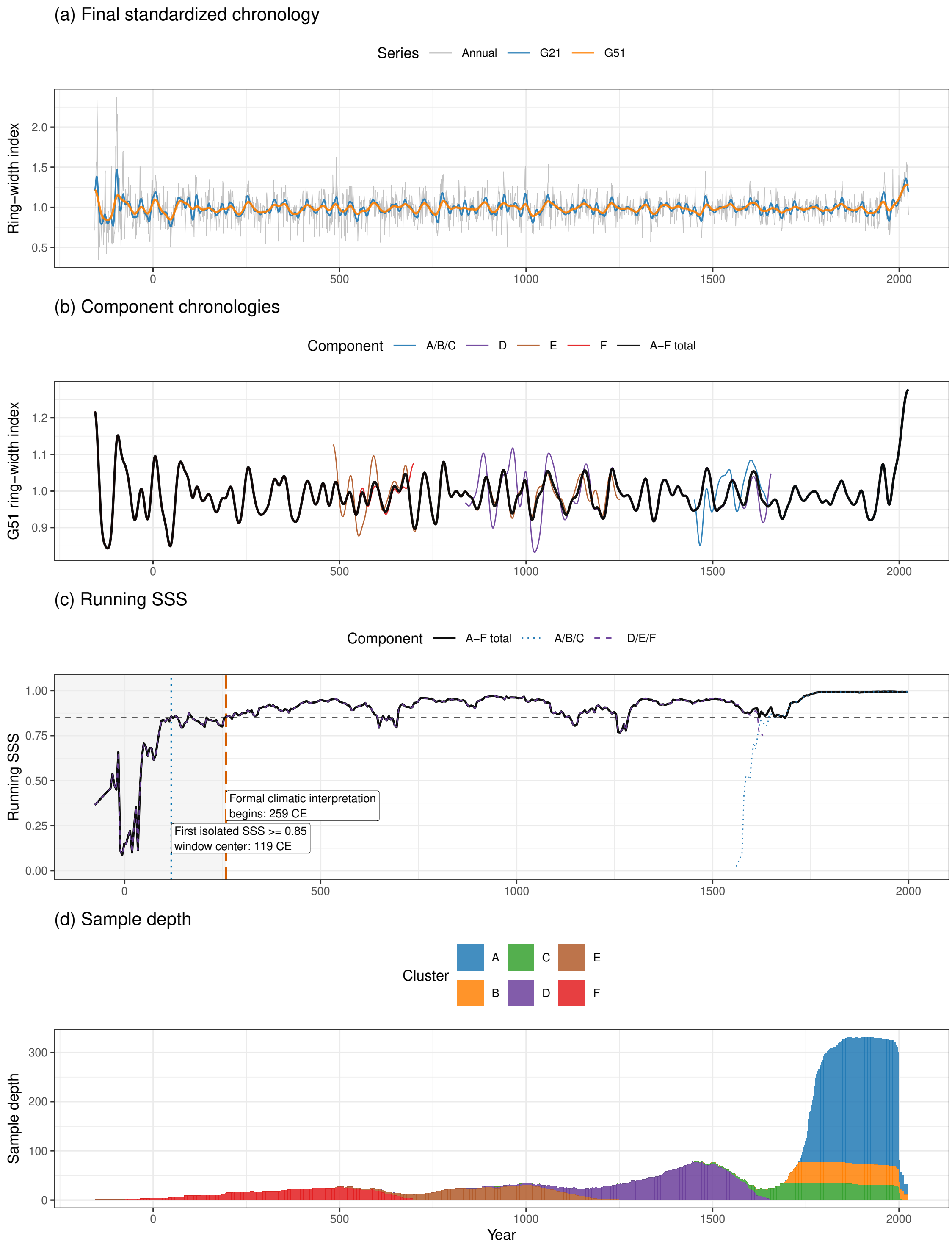

Figure S1: Standardized chronology, component low-frequency chronologies, running subsample signal strength (SSS), and sample depth. The SSS panel distinguishes the first isolated centered 51-year window above the conventional SSS $=$ 0.85 screening value (119 CE) from the conservative author-defined boundary for formal climatic interpretation (259 CE). Neither date is an estimated climate changepoint, and interval-specific SSS remains relevant after 259 CE.

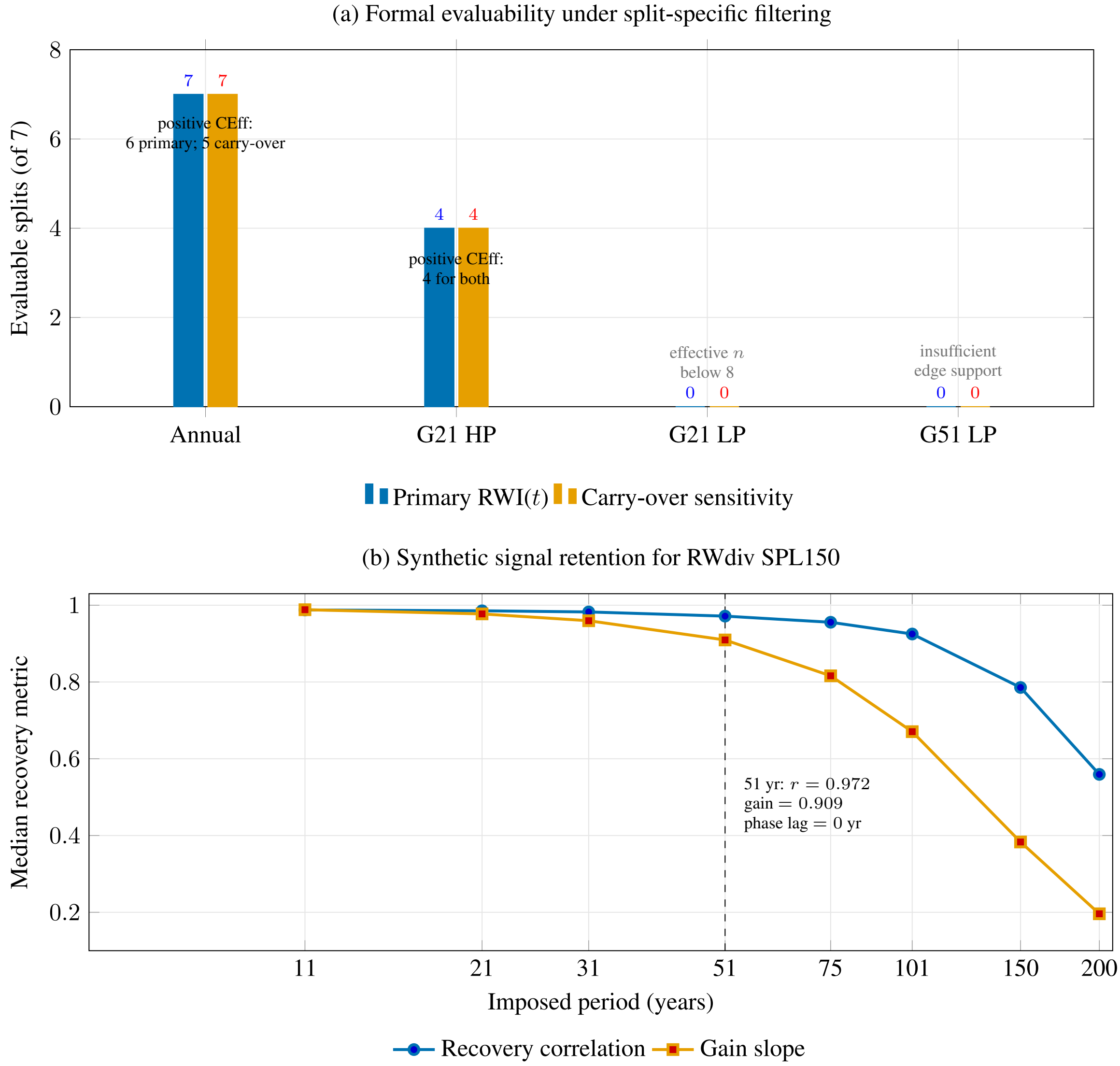

Figure S2: Formal evaluability of frequency-dependent verification and synthetic signal retention. Panel (a) gives the number of the seven predefined splits that remain evaluable after calibration and verification segments are filtered independently. Annual results are evaluable for all splits and G21 high-pass results for four; G21 and G51 low-pass results are not formally evaluable. Panel (b) shows median recovery correlation and gain for imposed signals passed through the selected RWdiv SPL150 chronology workflow. The vertical line marks 51 years. These transfer-response tests assess signal preservation, not climate predictive skill.

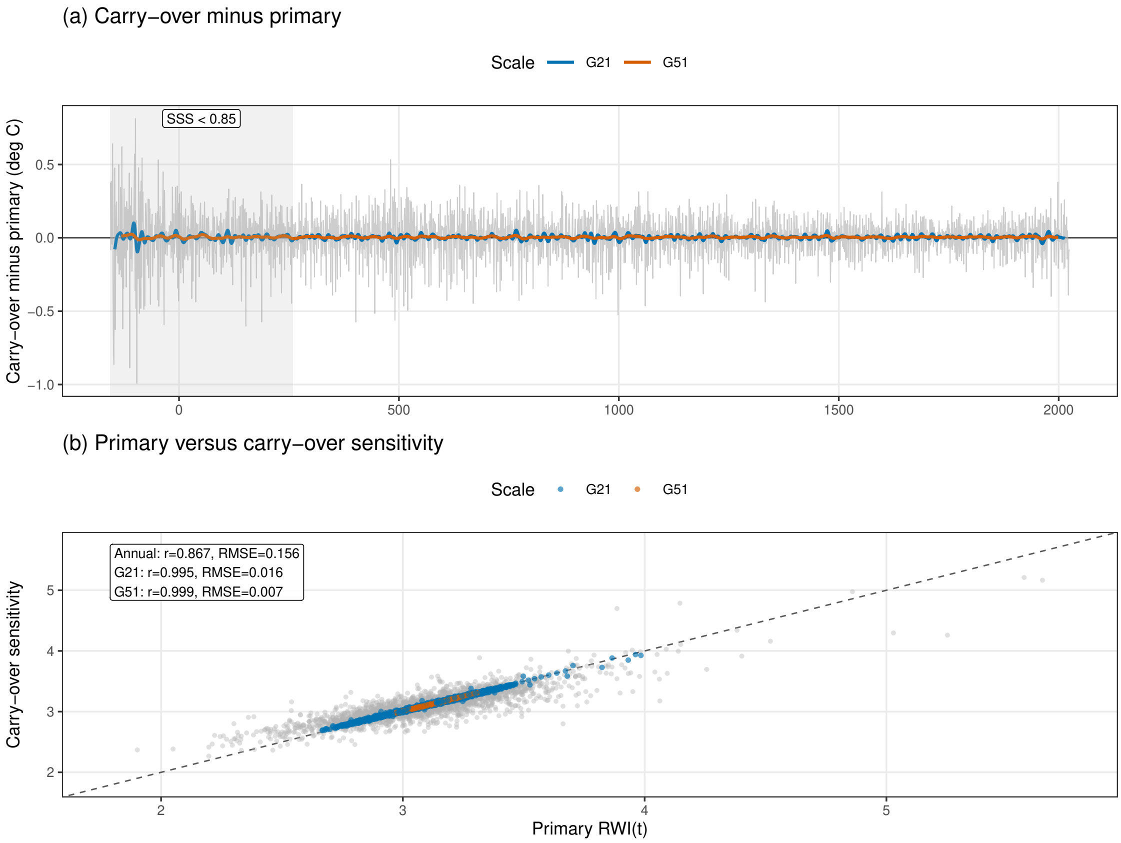

Figure S3: Carry-over sensitivity for the pNov–Apr reconstruction. The primary RWI(t) reconstruction is compared with the constrained mean[RWI(t), RWI($t+1$)] formulation. The comparison tests target-year assignment and does not replace the primary model.

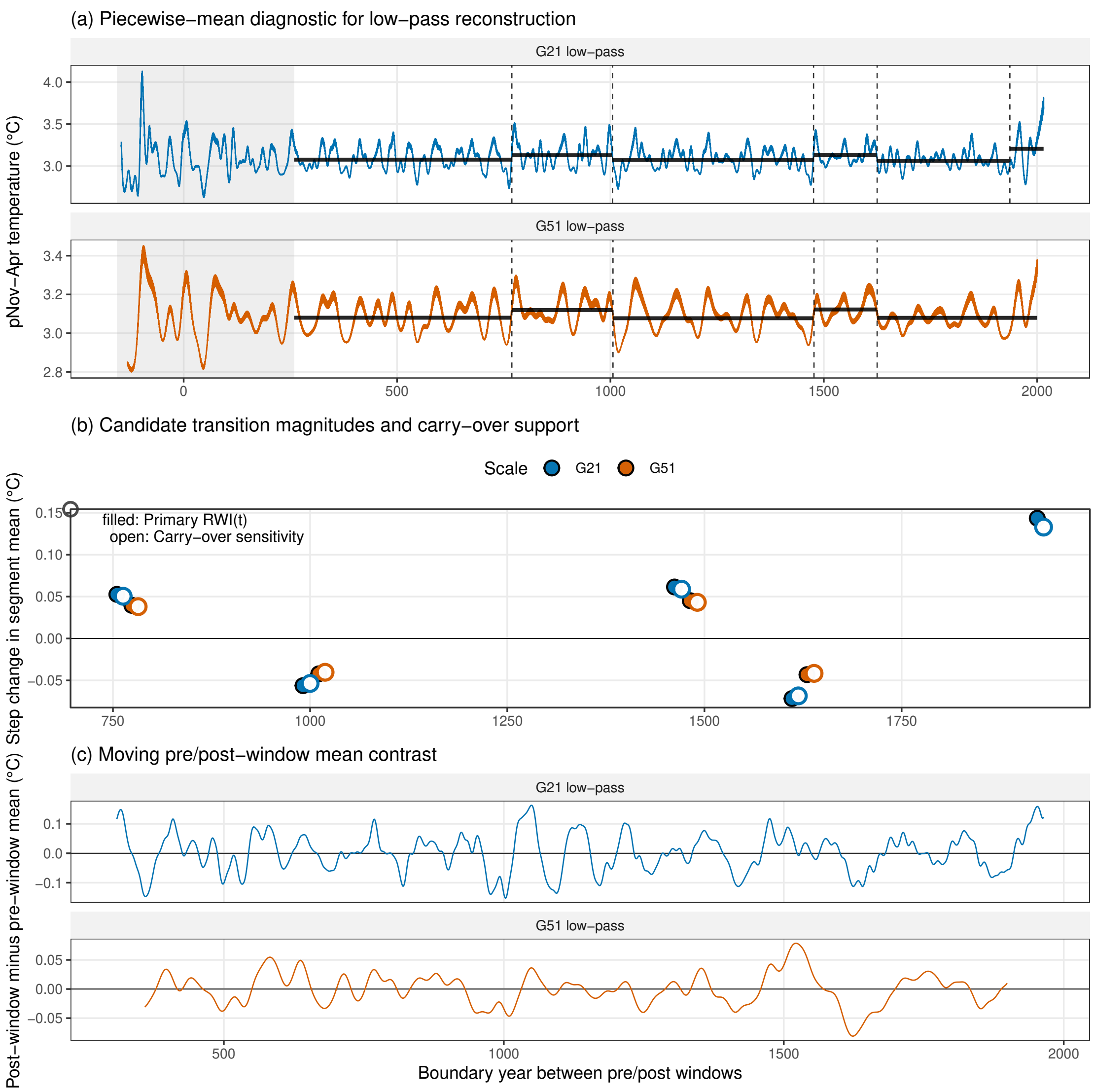

Figure S4: Descriptive smoothed-mean contrasts. The analysis locates large before–after differences in smoothed reconstructions but does not estimate formal regime shifts, candidate intervals, periodicity, or forcing.

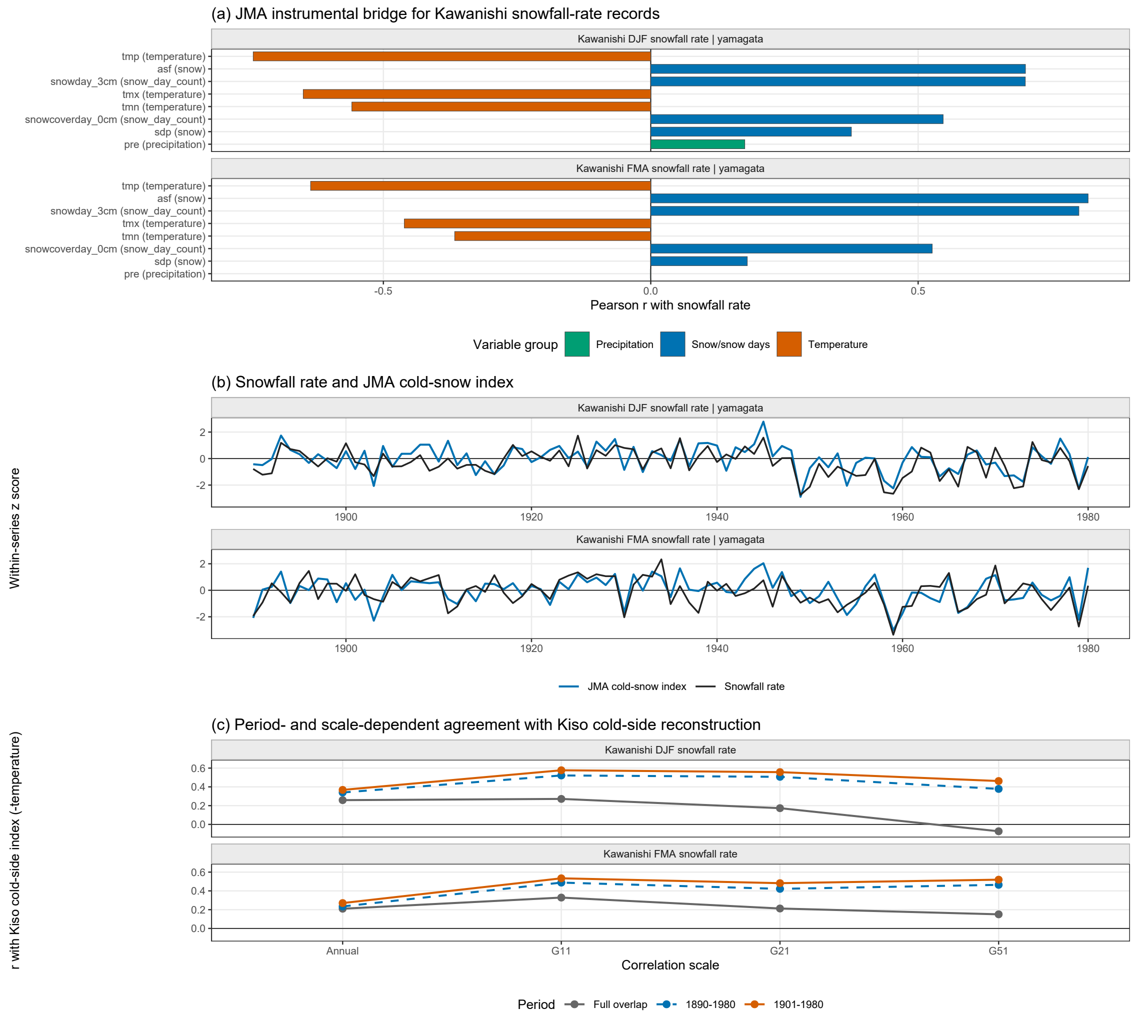

Figure S5: Kawanishi documentary snowfall-rate context. Panel (a) summarizes correlations with JMA Yamagata variables and establishes the local cold–snow meaning of the documentary rates. Panel (b) compares standardized snowfall-rate series with a JMA cold–snow index. Panel (c) shows annual and smoothed correlations between snowfall rate and the Kiso cold-side reconstruction for the full overlap and instrumental subperiods. The documentary series is used as regional context and is not an independent calibration or validation target.

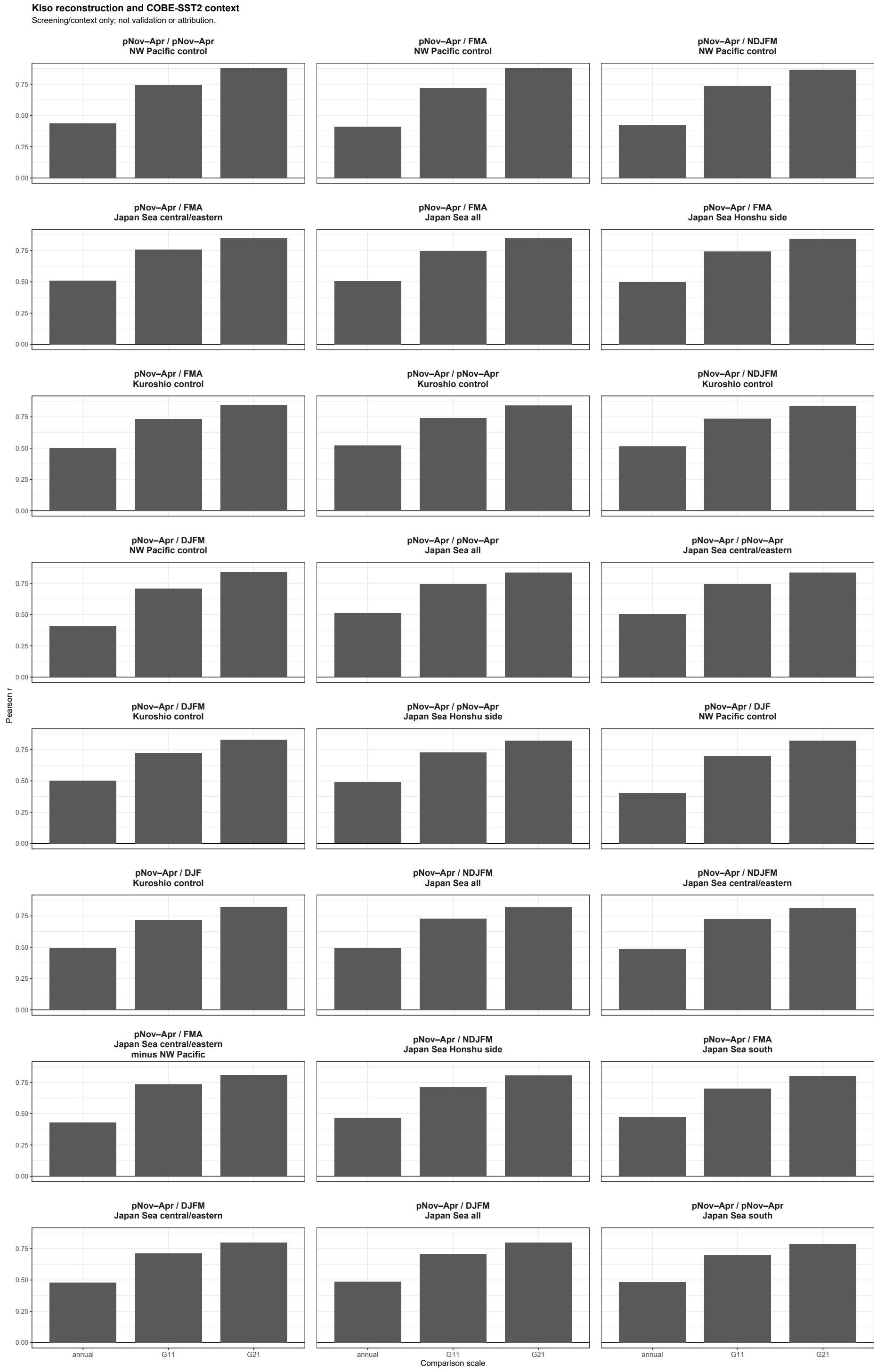

Figure S6: COBE-SST2 context for the Kiso pNov–Apr reconstruction. The displayed bar panels summarize Pearson correlations with selected SST boxes at annual, G11, and G21 comparison scales. The Siberian High and East Asian winter monsoon index results are reported in Table S7 and the accompanying text rather than as separate figure panels. All comparisons are screening and context diagnostics only; they are not independent validation or attribution to a single oceanic or atmospheric driver.

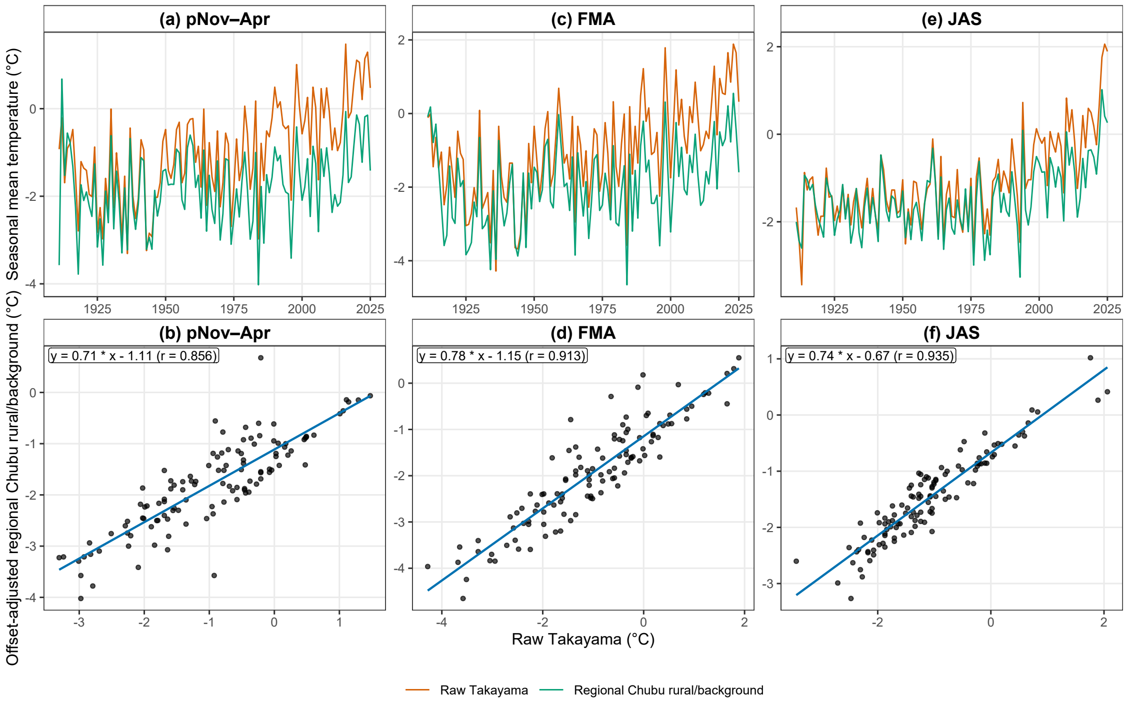

Figure S7: Raw Takayama station temperatures and offset-aligned regional rural/background Chubu targets. Panels (a), (c), and (e) show seasonal time series for pNov–Apr, FMA, and JAS; panels (b), (d), and (f) show the ordinary least-squares regressions used to quantify their relationship. The Chubu product incorporates eight rural/background stations. A season-specific additive offset was applied only for direct mean-level display. It does not affect variance, correlation, or the OLS slope within a specified regression direction; mean differences depend on the chosen alignment and are not interpreted as direct urban heat-island estimates. Machine-readable Tables S8g–S8i provide the full regression statistics, seasonal values, and raw Takayama climatology.

References

Bretherton, C. S., Widmann, M., Dymnikov, V. P., Wallace, J. M., and Bladé, I.: The Effective Number of Spatial Degrees of Freedom of a Time-Varying Field, Journal of Climate, 12, 1990–2009, https://doi.org/10.1175/1520-0442(1999)012<1990:TENOSD>2.0.CO;2, 1999.

D'Arrigo, R., Jacoby, G., Wilson, R., and Panagiotopoulos, F.: A reconstructed Siberian High index since A.D. 1599 from Eurasian and North American tree rings, Geophysical Research Letters, 32, L05 705, https://doi.org/10.1029/2004GL022271, 2005a.

D'Arrigo, R., Wilson, R., Panagiotopoulos, F., and Wu, B.: On the long-term interannual variability of the East Asian winter monsoon, Geophysical Research Letters, 32, L21 706, https://doi.org/10.1029/2005GL023235, 2005b.

Hirahara, S., Ishii, M., and Fukuda, Y.: Centennial-scale sea surface temperature analysis and its uncertainty, Journal of Climate, 27, 57–75, https://doi.org/10.1175/JCLI-D-12-00837.1, 2014.

Hirano, J., Ohba, T., Morishima, W., and Mikami, T.: Reconstruction of winter temperature since the 1830s in Kawanishi based on historical weather documents, Geographical Review of Japan Series A, 85, 275–286, in Japanese with English abstract, 2012.

Hirano, J., Hasegawa, N., Zaiki, M., and Mikami, T.: Long-term variations of snowfall ratio in the Sea of Japan side area of the Tohoku region since the late 17th century, Journal of Geography (Chigaku Zasshi), 134, 429–438, https://doi.org/10.5026/jgeography.134.429, in Japanese with English abstract, 2025.

Jeong, J.-H., Ou, T., Linderholm, H. W., Kim, B.-M., Kim, S.-J., Kug, J.-S., and Chen, D.: Recent recovery of the Siberian High intensity, Journal of Geophysical Research: Atmospheres, 116, D23 102, https://doi.org/10.1029/2011JD015904, 2011.

Katata, G. and Fujibe, F.: Monthly Background/Rural Air Temperature Data in Japan (1916–2023), https://doi.org/10.24567/0002006246, [data set], 2026.

Katata, G., Connolly, R., and O'Neill, P.: Evidence of Urban Blending in Homogenized Temperature Records in Japan and in the United States: Implications for the Reliability of Global Land Surface Air Temperature Data, Journal of Applied Meteorology and Climatology, 62, 1095–1114, https://doi.org/10.1175/JAMC-D-22-0122.1, 2023.

Katata, G., Nakayama, R., Fujibe, F., and Maeda, S.: Reconstruction of the Background Air Temperature Record in Japan (1916–2023): Implications for Climate Change and Urbanisation Bias in the 20th Century, International Journal of Climatology, 45, e70 141, https://doi.org/10.1002/joc.70141, 2025.

Ma, T. and Chen, W.: Climate variability of the East Asian winter monsoon and associated extratropical–tropical interaction: a review, Annals of the New York Academy of Sciences, 1504, 44–62, https://doi.org/10.1111/nyas.14620, 2021.

Ma, T. and Chen, W.: Recent progress in understanding the interaction between ENSO and the East Asian winter monsoon: a review, Frontiers in Earth Science, 11, 1098 517, https://doi.org/10.3389/feart.2023.1098517, 2023.

Miao, J. and Wang, T.: Decadal variations of the East Asian winter monsoon in recent decades, Atmospheric Science Letters, 21, e960, https://doi.org/10.1002/asl.960, 2020.

Ohyama, M., Yonenobu, H., Choi, J.-N., Park, W.-K., Hanzawa, M., and Suzuki, M.: Reconstruction of northeast Asia spring temperature 1784–1990, Climate of the Past, 9, https://doi.org/10.5194/cp-9-261-2013, 2013.

Ohyama, M., Yonenobu, H., Hoshino, Y., and Suzuki, S.: A two-millennia provenance-assured Chamaecyparis tree-ring chronology for central Japan, Dendrochronologia, 95, 126 461, https://doi.org/10.1016/j.dendro.2025.126461, 2026a.

Ohyama, M., Yonenobu, H., Hoshino, Y., and Suzuki, S.: Tree-ring_chronology_CJH25, https://doi.org/10.50974/0002007851, [data set], 2026b.

Panagiotopoulos, F., Shahgedanova, M., Hannachi, A., and Stephenson, D. B.: Observed trends and teleconnections of the Siberian High: A recently declining center of action, Journal of Climate, 18, 1411–1422, https://doi.org/10.1175/JCLI3352.1, 2005.

Song, M., Yang, B., Ljungqvist, F. C., Shi, F., Qin, C., and Wang, J.: Tree-ring-based winter temperature reconstruction for East Asia over the past 700 years, Science China Earth Sciences, 64, 872–889, https://doi.org/10.1007/s11430-020-9768-9, 2021.

Takaya, K. and Nakamura, H.: Interannual variability of the East Asian winter monsoon and related modulations of the planetary waves, Journal of Climate, 26, 9445–9461, https://doi.org/10.1175/JCLI-D-12-00842.1, 2013.

Tokoro, M.: Kinsei Ringyo-shi no Kenkyu (Study on the History of Early Modern Forestry), Yoshikawa Kobunkan, Tokyo, ISBN 978–4–642–042505, in Japanese, 1980.

Wigley, T. M. L., Briffa, K. R., and Jones, P. D.: On the average value of correlated time series, with applications in dendroclimatology and hydrometeorology, Journal of Applied Meteorology and Climatology, 23, 201–213, https://doi.org/10.1175/1520-0450(1984)023<0201:otavoc>2.0.co;2, 1984.

Yonenobu, H. and Eckstein, D.: Reconstruction of early spring temperature for central Japan from the tree-ring widths of Hinoki cypress and its verification by other proxy records, Geophysical Research Letters, 33, https://doi.org/10.1029/2006gl026170, 2006.

Yonenobu, H., Nagai, A., Ohyama, M., and Hoshino, Y.: A ring-width reference chronology of Nezuko/Kurobe (Thuja standishii (Gordon) Carrière, Cupressaceae) from the Kiso Mountains, central Japan, Japanese Journal of Historical Botany, 35, 35–44, 2026.

Zhu, H. F., Fang, X. Q., Shao, X. M., and Yin, Z. Y.: Tree ring-based February–April temperature reconstruction for Changbai Mountain in Northeast China and its implication for East Asian winter monsoon, Climate of the Past, 5, 661–666, https://doi.org/10.5194/cp-5-661-2009, 2009.